

Supporting Information

Mononuclear Nonheme Iron(IV)-Oxo and Manganese(IV)-Oxo Complexes in Oxidation Reactions: Experimental Results Prove Theoretical Prediction

Junying Chen,[‡] Kyung-Bin Cho,[‡] Yong-Min Lee, Yoon Hye Kwon, and Wonwoo Nam*

*Department of Chemistry and Nano Science, Center for Biomimetic Systems, Ewha Womans
University, Seoul 120–750, Korea*

*E-mail: wwnam@ewha.ac.kr (W.N.)

[‡] These authors contributed equally to this study.

Table of Contents

Experimental Section	S3
Materials	S3
Instrumentation	S3
Kinetic Studies	S3
References (Experimental Section)	S3
Table S1	S5
Table S2	S6
Fig. S1	S7
Fig. S2	S8
Fig. S3	S9
Fig. S4	S10
Fig. S6	S11
Fig. S7	S12
Fig. S8	S13
DFT Calculations Section	S14
Methods	S14
Free Energy Calculations	S14
Electron Rearrangement for $S = 1/2$ Fe ^{IV} O Sulfoxidation Reaction	S15
Orbital Discussions for Sulfoxidation Reaction	S15
Fig. S5	S17
References (DFT Section)	S18
Tables for Energies (Tables S3 – S8)	S19
Tables for Mulliken Spin Density Distribution (Tables S9 – S14)	S24
Tables for Geometries (Tables S15 – S20)	S27
DFT Coordinates	S30

Experimental Section

Materials. Commercially available chemicals were used without further purification unless otherwise indicated. Solvents were dried according to published procedures and distilled under Ar prior to use.^{S1} H₂¹⁸O (95% ¹⁸O-enriched) was purchased from ICON Services Inc. (Summit, NJ, USA). Iodosylbenzene (PhIO), N4Py ligand, [Fe^{II}(N4Py)](CF₃SO₃)₂ and [Mn^{II}(N4Py)](CF₃SO₃)₂ complexes were prepared according to the reported methods.^{S2-S7}

Instrumentation. UV-vis spectra were recorded on a Hewlett Packard 8453 diode array spectrophotometer equipped with a UNISOKU Scientific Instruments Cryostat USP-203A for low-temperature experiments or on a Hi-Tech Scientific (U.K.) SF-61 DX2 cryogenic stopped-flow spectrophotometer equipped with a Xe arc lamp and a KinetaScan diode array rapid scanning unit.

Kinetic Studies. Kinetic measurements were performed on a UV-vis spectrophotometer or a stopped-flow spectrophotometer in CF₃CH₂OH-CH₃CN (*v/v* = 19:1) at 273 K for OAT reactions and 298 K for C-H bond activation reactions. Oxidations of substrates by **1** and **2** were performed by monitoring spectral changes at 695 nm for **1** and at 940 nm for **2**, respectively, with various concentrations of substrates. The concentration of substrates was at least more than 10-fold excess of **1** or **2** to attain pseudo-first-order reaction conditions. First-order fitting of the kinetic data allowed us to determine the pseudo-first-order rate constants. The first-order plots were linear for three or more half-lives with the correlation coefficient of $\rho > 0.999$. In each case, it was confirmed that the rate constants derived from at least five independent measurements agreed within an experimental error of $\pm 10\%$. The pseudo-first-order rate constants increased proportionally with the concentrations of substrates, from which second-order rate constants were determined.

References (Experimental section)

- S1. W. L. F. Armarego and C. L. L. Chai, *Purification of Laboratory Chemicals*, 6th ed.; Pergamon Press: Oxford, 2009.
- S2. O. Bortolini, S. Campestrini, F. Di Furia and G. Modena, *J. Org. Chem.*, 1987, **52**, 5093.
- S3. J. Kaizer, E. J. Klinker, N. Y. Oh, J.-U. Rohde, W. J. Song, A. Stubna, J. Kim, E. Münck, W. Nam and L. Que, Jr, *J. Am. Chem. Soc.*, 2004, **126**, 472.

- S4. H. Saltzman and J. G. Sharefkin, Eds.; *Organic Syntheses*; Wiley: New York, 1973, Vol. V, p 658.
- S5. N. E. Dixon, G. A. Lawrance, P. A. Lay, A. M. Sargeson and H. Taube, *Inorg. Synth.*, 1990, **28**, 70.
- S6. (a) M. Lubben, A. Meetsma, E. C. Wilkinson, B. Feringa and L. Que, Jr, *Angew. Chem., Int. Ed.*, 1995, **34**, 1512; (b) L. Duelund, R. Hazell, C. J. McKenzie, L. P. Nielsen and H. Toftlund, *J. Chem. Soc., Dalton Trans.*, 2001, 152; (c) S. Groni, P. Dorlet, G. Blain, S. Bourcier, R. Guillot and E. Anxolabéhère-Mallart, *Inorg. Chem.*, 2008, **47**, 3166.
- S7. (a) J. Chen, Y.-M. Lee, K. M. Davis, X. Wu, M. S. Seo, K.-B. Cho, H. Yoon, Y. J. Park, S. Fukuzumi, Y. N. Pushkar and W. Nam, *J. Am. Chem. Soc.*, 2013, **135**, 6388; (b) H. Yoon, Y.-M. Lee, X. Wu, K.-B. Cho, R. Sarangi, W. Nam and S. Fukuzumi, *J. Am. Chem. Soc.*, 2013, **135**, 9186; (c) X. Wu, M. S. Seo, K. M. Davis, Y.-M. Lee, J. Chen, K.-B. Cho, Y. N. Pushkar and W. Nam, *J. Am. Chem. Soc.*, 2011, **133**, 20088; (d) H. Yoon, Y. Morimoto, Y.-M. Lee, W. Nam and S. Fukuzumi, *Chem. Commun.*, 2012, **48**, 11187.

Table S1. Second-order rate constants (k_2) determined in the oxidation reactions of hydrocarbons by $[\text{Fe}^{\text{IV}}(\text{O})(\text{N4Py})]^{2+}$ (**1**) and $[\text{Mn}^{\text{IV}}(\text{O})(\text{N4Py})]^{2+}$ (**2**).^a

substrate	BDE ^b kcal mol ⁻¹	1	2
		$k_2, \text{M}^{-1} \text{s}^{-1}$	$k_2, \text{M}^{-1} \text{s}^{-1}$
DHA	77	93(7)	8.9(6)
CHD	78	64(5)	6.2(4)
fluorene	80	3.3(3)	$2.9(2) \times 10^{-1}$
cumene	85	$1.5(1) \times 10^{-1}$	$6.8(4) \times 10^{-3}$
ethylbenzene	87	$5.5(3) \times 10^{-2}$	$4.4(4) \times 10^{-3}$
toluene	90	$4.8(4) \times 10^{-3}$	

^a Reaction conditions: in $\text{CF}_3\text{CH}_2\text{OH}-\text{CH}_3\text{CN}$ ($v/v = 19:1$) at 298 K

^b Taken from reference 18 in Text.

Table S2. Second-order rate constants (k_2) determined in the oxidation reactions of *para*-X-thioanisoles by **1** and **2**.^a

X in <i>para</i> -X-thioanisole	σ_p	E_{ox} V vs. SCE ^b	1	2^b
			$k_2, \text{M}^{-1} \text{s}^{-1}$	$k_2, \text{M}^{-1} \text{s}^{-1}$
MeO	-0.27	1.18	7.6(5)	$4.0(3) \times 10^{-1}$
Me	-0.17	1.27	3.1(3)	$5.0(4) \times 10^{-2}$
H	0.00	1.37	1.1(1)	$9.2(7) \times 10^{-3}$
F	0.062	1.40	$6.3(4) \times 10^{-1}$	$7.6(4) \times 10^{-3}$
Br	0.23	1.46	$9.7(8) \times 10^{-2}$	$1.6(2) \times 10^{-3}$

^a Reaction conditions: in CF₃CH₂OH-CH₃CN ($v/v = 19:1$) at 273 K

^b Taken from reference 10 in Text.

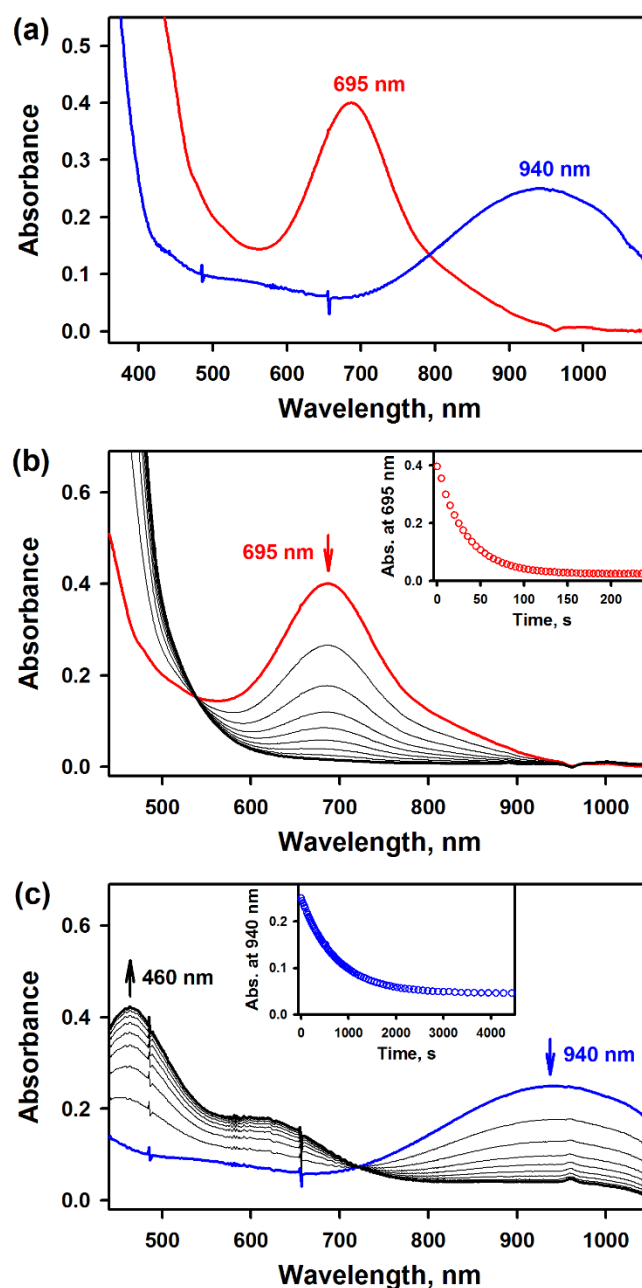


Fig. S1 (a) UV-vis spectra of **1** (red line) and **2** (blue line) in $\text{CF}_3\text{CH}_2\text{OH}-\text{CH}_3\text{CN}$ ($v/v = 19:1$) at 298 K. (b) UV-vis spectral changes observed in the reaction of **1** (1.0 mM, red line) and cumene (20 mM) in $\text{CF}_3\text{CH}_2\text{OH}-\text{CH}_3\text{CN}$ ($v/v = 19:1$) at 298 K. Inset shows the time course monitored at 695 nm due to **1**. (c) UV-vis spectral changes observed in the reaction of **2** (1.0 mM, blue line) and cumene (20 mM) in $\text{CF}_3\text{CH}_2\text{OH}-\text{CH}_3\text{CN}$ ($v/v = 19:1$) at 298 K. Inset shows the time course monitored at 940 nm due to **2**.

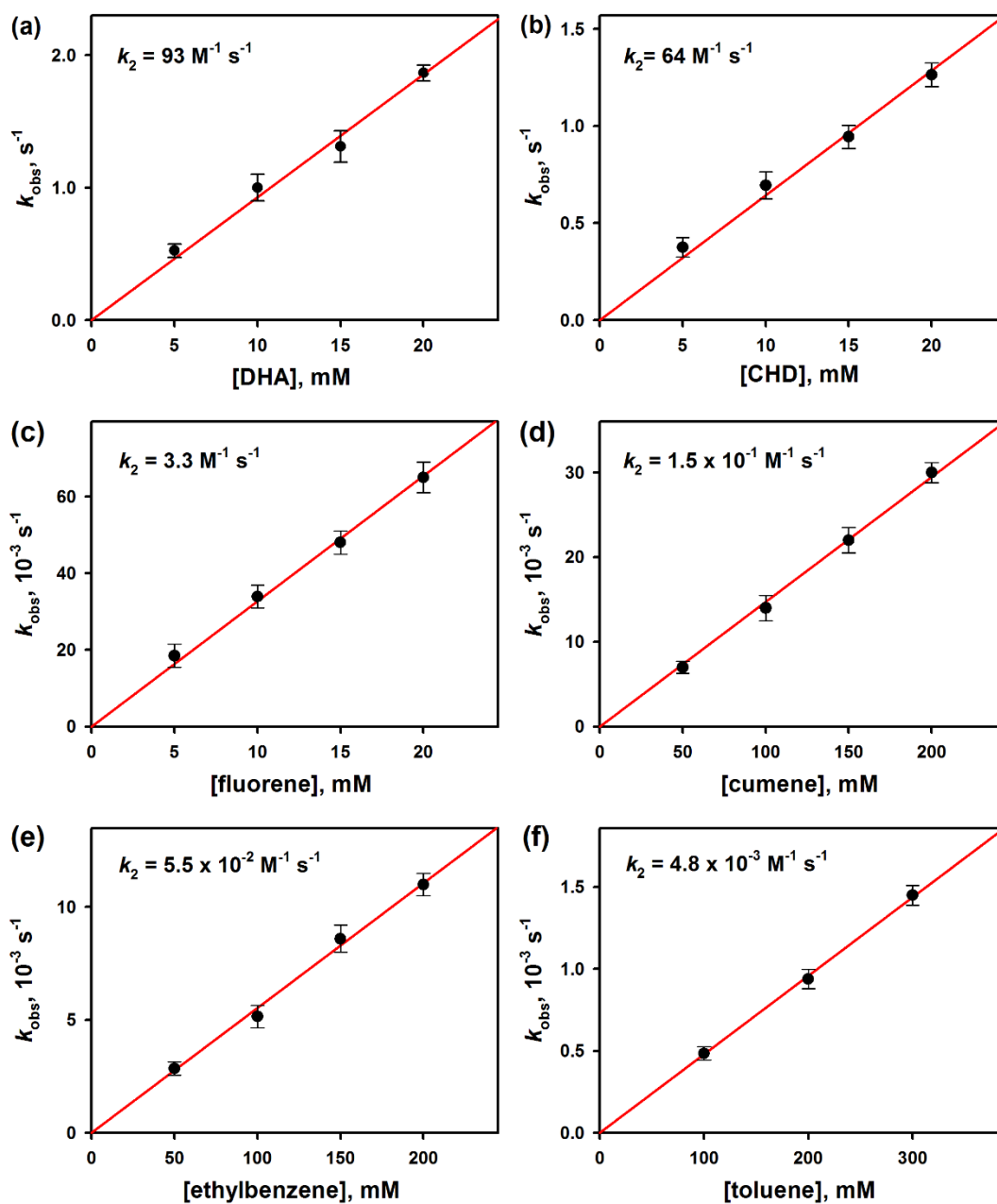


Fig. S2 Plots of the pseudo-first-order rate constants (k_{obs}) against substrate concentrations to determine second-order rate constants (k_2) for the oxidation reactions of (a) 9,10-dihydroanthracene (DHA), (b) 1,4-cyclohexadiene (CHD), (c) fluorene, (d) cumene, (e) ethylbenzene, and (f) toluene by **1** in $\text{CF}_3\text{CH}_2\text{OH}-\text{CH}_3\text{CN}$ ($v/v = 19/1$) at 298 K.

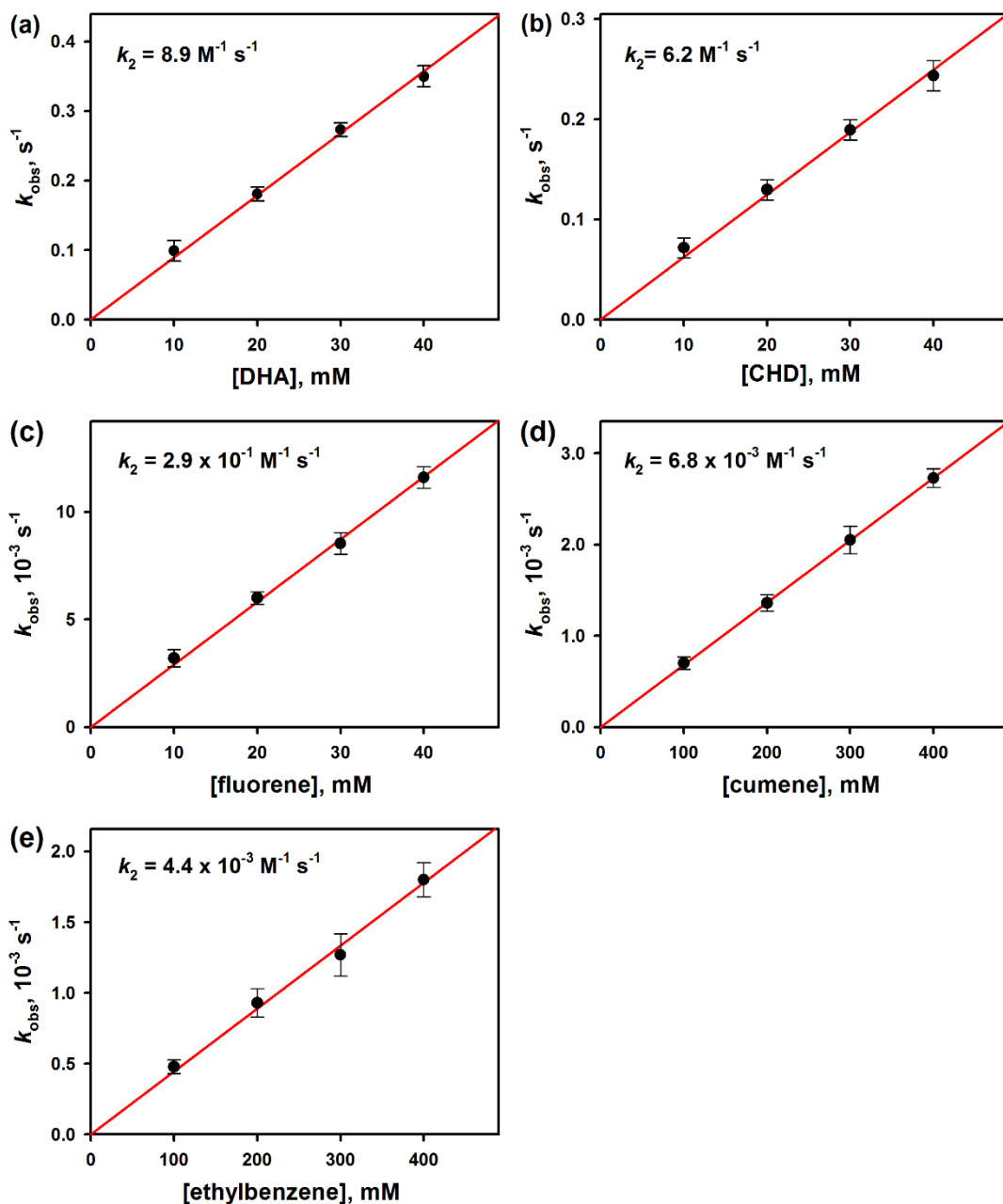


Fig. S3 Plots of the pseudo-first-order rate constants (k_{obs}) against substrate concentrations to determine second-order rate constants (k_2) for the oxidation reactions of (a) 9,10-dihydroanthracene (DHA), (b) 1,4-cyclohexadiene (CHD), (c) fluorene, (d) cumene, and (e) ethylbenzene by **2** in $\text{CF}_3\text{CH}_2\text{OH}-\text{CH}_3\text{CN}$ ($v/v = 19:1$) at 298 K.

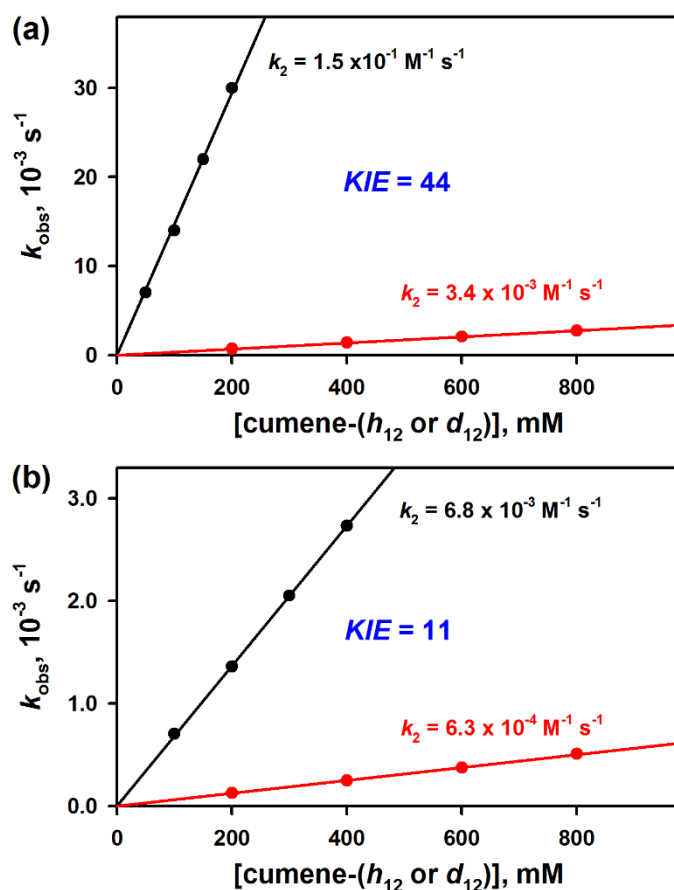


Fig. S4 (a) Plots of the first-order rate constants (k_{obs}) against substrate concentrations to determine second-order rate constants (k_2) and KIE value in the oxidation reactions of cumene- h_{12} (black circles) and cumene- d_{12} (red circles) by **1** in $\text{CF}_3\text{CH}_2\text{OH}-\text{CH}_3\text{CN}$ ($v/v = 19:1$) at 298 K. (b) Plots of the first-order rate constants (k_{obs}) against substrate concentrations to determine second-order rate constants (k_2) and KIE value in the oxidation reactions of cumene- h_{12} (black circles) and cumene- d_{12} (red circles) by **2** in $\text{CF}_3\text{CH}_2\text{OH}-\text{CH}_3\text{CN}$ ($v/v = 19:1$) at 298 K.

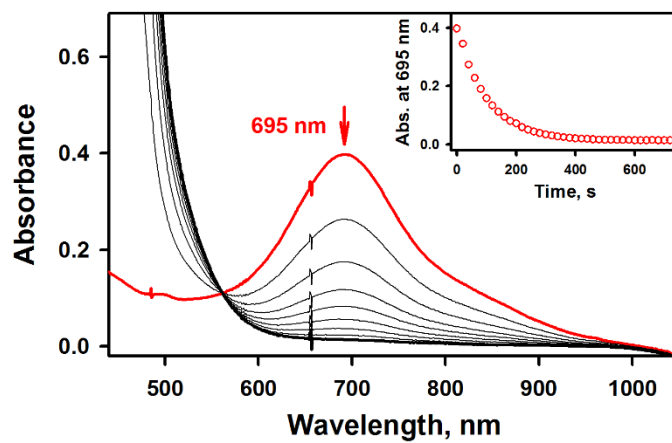


Fig. S6 UV-vis spectral changes observed in the reaction of **1** (1.0 mM, red line) and *para*-Br-thioanisole (0.10 M) in CF₃CH₂OH-CH₃CN ($v/v = 19:1$) at 273 K. Inset shows the time course monitored at 695 nm due to **1**.

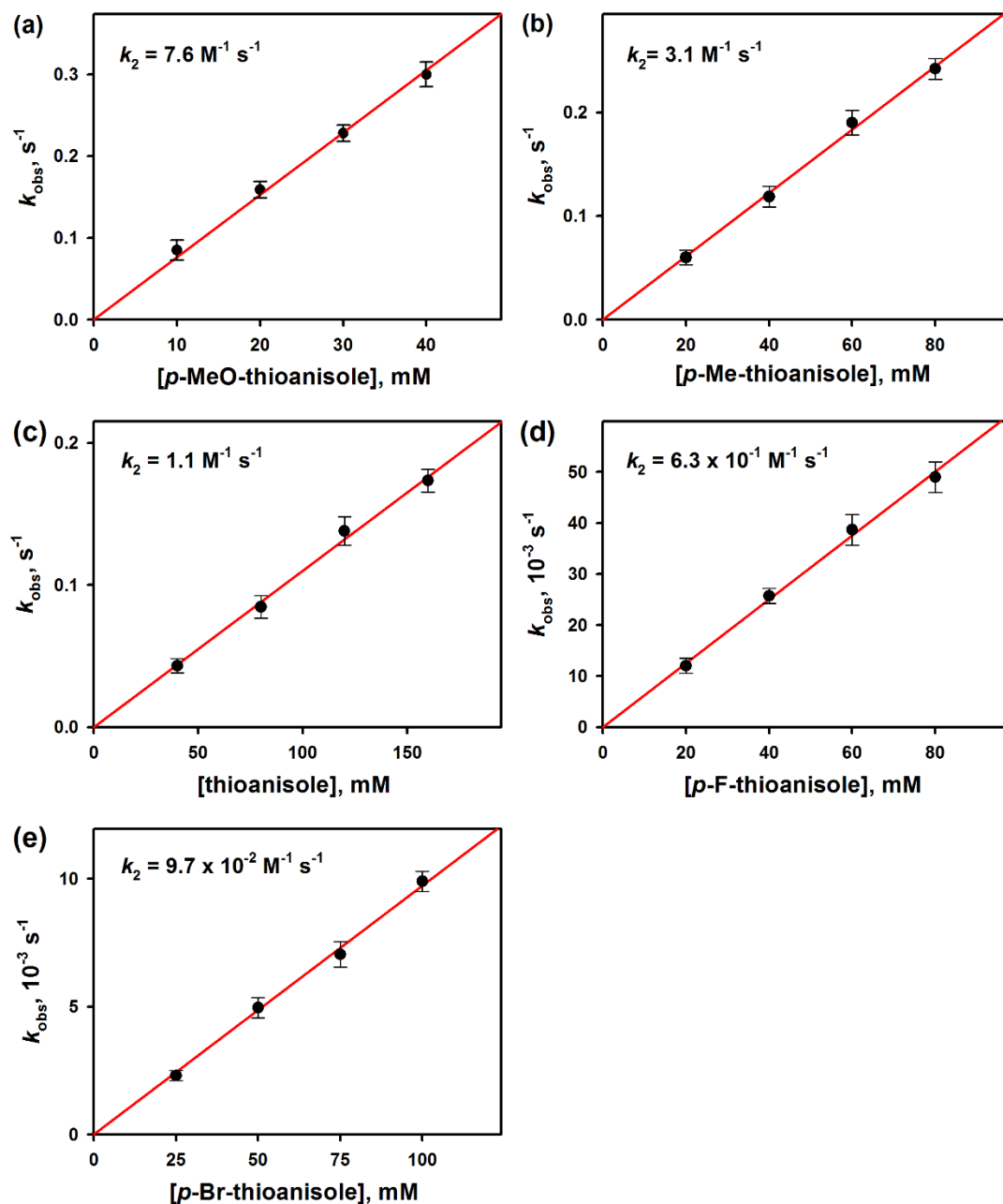


Fig. S7 Plots of the pseudo-first-order rate constants (k_{obs}) against substrate concentrations to determine second-order rate constants (k_2) for the oxidation reactions of *para*-X-thioanisole derivatives (X = (a) OMe, (b) Me, (c) H, (d) F, and (e) Br) by **1** with in $\text{CF}_3\text{CH}_2\text{OH}-\text{CH}_3\text{CN}$ ($v/v = 19:1$) at 273 K.

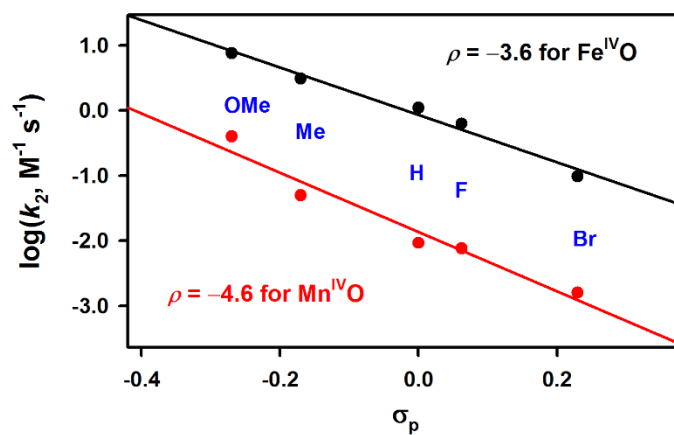


Fig. S8 Hammett plots of the $\log k_2$ against σ_p of *para*-X-thioanisole derivatives (X = OMe, Me, H, F and Br) by **1** (black circles) and **2** (red circles) in $\text{CF}_3\text{CH}_2\text{OH}-\text{CH}_3\text{CN}$ ($v/v = 19:1$) at 273 K.

Density Functional Theory Calculations

Methods. Density functional theory (DFT)^{S8} was applied using the B3LYP functional^{S9} as implemented in the Gaussian 09 (G09) package.^{S10} The geometries were optimized using the LACVP basis set, which uses Los Alamos ECP on transition metals^{S11} (slightly tweaked as implemented in the Jaguar program),^{S12} and 6-31G on the rest of the atoms.^{S13} In the sulfoxidation reactions, a polarization function was added (i.e. 6-31G*) to the S and O atoms as the sulphur is known to require a larger optimization basis set to yield correct bond lengths. The stationary states were confirmed by frequency calculations, and the transition states were connected with the ground states on both sides by performing IRC calculations and continuing relaxing the geometry down to ground state from the end geometry obtained by IRC. The high molecular charge (2+) made it necessary to perform the optimizations in solvent to avoid artificial results (*vide infra*).^{S14} The solvent (acetonitrile) effects were included using CPCM model with UFF cavity, per G09 default.^{S15} Single-point energy evaluations on the optimized geometry were done with the LACV3P** basis set.^{S12} This resulting electronic energy (ΔE) was used throughout the text as the final energy due to sufficient accuracy (*vide infra*).

Free Energy Calculations. Free energy calculations were done and presented in the ESI tables below, albeit not used in the text (*vide infra*). Dispersion effects were calculated using DFT-D3 program.^{S16} MECP was found using a shell program to G09 that iterates to the same energy and geometry for two different spin states.^{S17} The instable excited state of Mn^{IV}O was obtained using less strict convergence criteria on the SCF iterations (10^{-5} in accuracy instead of the G09 default of 10^{-10}) during the geometry optimizations using LACVP. Therefore, the energy value of this state is an upper limit value, which is notably still lower than the other TS values.

In previous trials, we have found that using gas-phase optimizations in HAT reactions for highly charged species such as the current system (2+) can cause a hydride transfer (i.e. one proton and two electrons) rather than a net hydrogen atom transfer from the substrate to the metal-oxo species due to self-interaction errors (SIE). Most of the time, performing optimizations in solvent avoids these artificial results;^{S14} hence the solvent effects were included during optimizations. However, in doing so, other problems may arise. Adding thermal contributions then becomes in principle inaccurate since the standard solvent models are parameterized to yield good solvation free energies and not any other property. This means that thermal effects are already included, to a certain extent, in the obtained electronic energies, hence possibly double counting the thermal contributions^{S18} (the same consideration applies to the dispersion correction as well). On the other hand, gas-phase frequency calculations on the

so obtained structure may not be meaningful either since the structure may not be in a stationary point without the solvent. This leaves us in principle with no easily available options to calculate in a uniform manner the free energies and at the same time avoid SIE, for highly charge systems, unless one is prepared to enlarge the model system to include counter ions,^{S19} which may be more time consuming and sometimes leading to ‘reactions’ between the transition metal complex and the counter ions, which may or may not be realistic.

Assuming though that the above described errors are negligible, the free energies (ΔG) can still be calculated by adding zero-point vibration energy (ΔZ_0), thermal corrections to Z_0 and entropy $-T\Delta S$. Relatively recent consensus is that dispersion effects are needed as well (ΔDisp). Also, if the energy of separated reactants in solvent is evaluated, there is a correction factor of $RT \cdot \ln(24.5)$ due to change of standard states (either subtracted from the complexed states or added to the non-complexed states, depending on the reference state).^{S20} In C-H activation reactions, tunnelling is an issue as well,^{S21} but is ignored in the current study since its magnitude is not likely to affect the main conclusions. If using separated reactants as the reference point, it is our experience that ΔDisp are usually large, but is roughly cancelled out by $-T\Delta S$. At the same time, $\Delta Z_0 + RT \cdot \ln(24.5)$ is roughly cancelled out by thermal corrections to Z_0 and complexation energy together. Hence, basing the relative energies on ΔE with the complexed reactants as the reference point gives as many times the same values (within some error margins) as free energies ΔG with the separated reactants as the reference point, as evidenced by many, many early days DFT ΔE calculations that gave surprisingly good agreement with experiments without any corrections. Therefore, we use throughout this study the electronic energies (ΔE) without any correction factors (except for solvent modelling, which is included by default on all calculations) due to its simplicity, both in calculation and analysis. Our approach is ultimately validated by the good agreement with experiments, within the expected error margins ($\pm 3 \text{ kcal mol}^{-1}$).

Electron Rearrangement for $S = 1/2 \text{ Fe}^{\text{IV}}\text{O}$ Sulfoxidation Reaction. In the case of the sulfoxidation reaction by **1**, we found that the $S = 1/2$ reaction also reacts through excited state reactivity (ESR), similar to the Mn case (*vide infra*, Fig. S8). The electron in the π^*_{xz} orbital is transferred to the σ^*_{xy} orbital, forming a second reactant before the reaction. This second reactant structure was possible to obtain as the substrate is transferring about 0.5 in spin to π^*_{xz} already at this stage (Table S13), making the structure stable.

Orbital Discussions for Sulfoxidation Reaction. The transformation of the interacting orbitals during the sulfoxidation reaction can be easily understood if we divide the reaction in

two conceptual steps: the M-O bond dissociation and O-S bond formation. The valence orbitals in the MO moiety contains the anti-bonding orbitals σ^*_{z2} , σ^*_{xy} , π^*_{xz} and π^*_{xz} , with their bonding counterparts, σ_{z2} , σ_{xy} , π_{xz} and π_{xz} lower in energy. There is also an orbital, sometimes named δ , which is in fact the same as d_{xy} orbital. During the M-O bond dissociation, all the orbitals except δ and σ^*_{xy} (which do not consist of contributions from O) decompose to their contributing orbitals; hence σ_{z2} and σ^*_{z2} become d_{z2} on M and p_z on O, π_{yz} and π^*_{yz} become d_{yz} on M and p_y on O, and π_{xz} and π^*_{xz} become d_{xz} on M and p_x on O. Depending on the specific electron configuration, the sp^2 lone pair orbital on S can now choose to form a bonding (and anti-bonding) orbital with either p_x , which gives an ideal M-O-S geometry of 90° or it can interact with p_z through an 180° attack. Fig. S5 details the electron transfers for each of the species in this study.

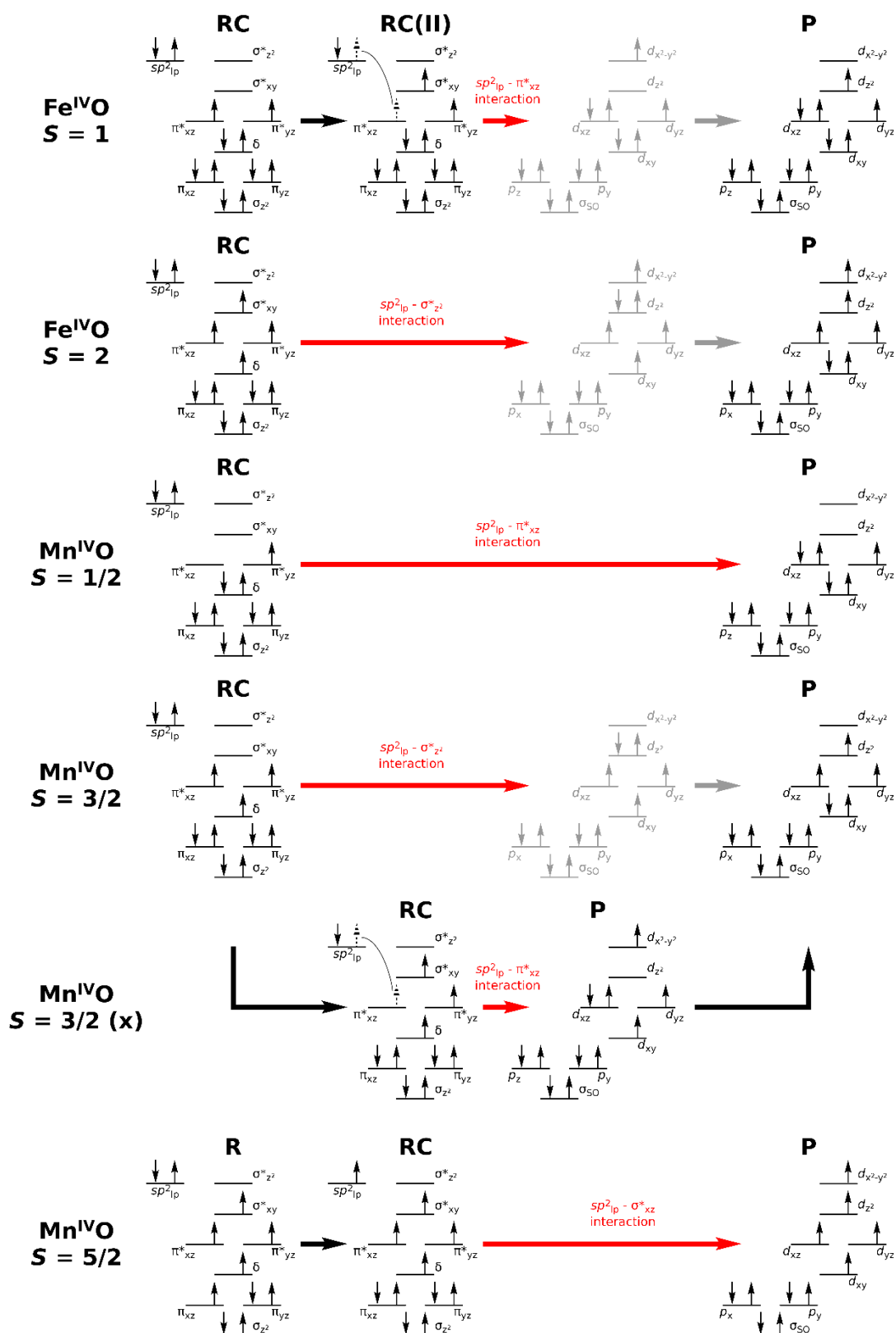


Fig. S5 Orbital transformations and electron occupation during sulfoxidation reactions by **1** and **2**. Red arrows mark the sulfoxidation step, which can be preceded or succeeded by an unstable state that is not the ground state. The grey configurations are postulated unstable states that was not obtained in this study.

References (DFT section)

- S8. W. Kohn and L. J. Sham, *Phys. Rev. A*, 1965, **140**, 1133.
- S9. (a) A. D. Becke, *Phys. Rev. A*, 1988, **38**, 3098; (b) A. D. Becke, *J. Chem. Phys.*, 1993, **98**, 1372; (c) A. D. Becke, *J. Chem. Phys.*, 1993, **98**, 5648; (d) C. Lee, W. T. Yang and R. G. Parr, *Phys. Rev. B*, 1988, **37**, 785.
- S10. M. J. Frisch, G. W. Trucks, H. B. Schlegel, G. E. Scuseria, M. A. Robb, J. R. Cheeseman, G. Scalmani, V. Barone, B. Mennucci, G. A. Petersson, H. Nakatsuji, M. Caricato, X. Li, H. P. Hratchian, A. F. Izmaylov, J. Bloino, G. Zheng, J. L. Sonnenberg, M. Hada, M. Ehara, K. Toyota, R. Fukuda, J. Hasegawa, M. Ishida, T. Nakajima, Y. Honda, O. Kitao, H. Nakai, T. Vreven, J. A. Montgomery, Jr., J. E. Peralta, F. Ogliaro, M. Bearpark, J. J. Heyd, E. Brothers, K. N. Kudin, V. N. Staroverov, T. Keith, R. Kobayashi, J. Normand, K. Raghavachari, A. Rendell, J. C. Burant, S. S. Iyengar, J. Tomasi, M. Cossi, N. Rega, J. M. Millam, M. Klene, J. E. Knox, J. B. Cross, V. Bakken, C. Adamo, J. Jaramillo, R. Gomperts, R. E. Stratmann, O. Yazyev, A. J. Austin, R. Cammi, C. Pomelli, J. W. Ochterski, R. L. Martin, K. Morokuma, V. G. Zakrzewski, G. A. Voth, P. Salvador, J. J. Dannenberg, S. Dapprich, A. D. Daniels, O. Farkas, J. B. Foresman, J. V. Ortiz, J. Cioslowski, and D. J. Fox, *Gaussian 09, Revisions B.01 and D.01*, Gaussian, Inc., Wallingford CT, 2010.
- S11. (a) P. J. Hay and W. R. Wadt, *J. Chem. Phys.*, 1985, **82**, 270; (b) P. J. Hay and W. R. Wadt, *J. Chem. Phys.*, 1985, **82**, 299.
- S12. Jaguar, version 7.7, Schrödinger, LLC, New York, NY, 2010.
- S13. (a) W. J. Hehre, R. Ditchfield and J. A. Pople, *J. Chem. Phys.*, 1972, **56**, 2257; (b) M. M. Francl, W. J. Pietro, W. J. Hehre, J. S. Binkley, M. S. Gordon, D. J. DeFrees and J. A. Pople, *J. Chem. Phys.*, 1982, **77**, 3654.
- S14. (a) A. J. Johansson, M. R. A. Blomberg, and P. E. M. Siegbahn, *J. Chem. Phys.*, 2008, **129**, 154301; (b) A. J. Johansson, M. R. A. Blomberg, and P. E. M. Siegbahn, *J. Phys. Chem. C*, 2007, **111**, 12397.
- S15. M. Cossi, N. Rega, G. Scalmani and V. Barone, *J. Comput. Chem.*, 2003, **24**, 669.
- S16. S. Grimme, J. Antony, S. Ehrlich, and H. Krieg, *J. Chem. Phys.*, 2010, **132**, 154104.
- S17. J. N. Harvey, M. Aschi, H. Schwarz and W. Koch, *Theor. Chem. Acc.*, 1998, **99**, 95.
- S18. J. Ho, A. Klamt and M. L. Coote, *J. Phys. Chem. A*, 2010, **114**, 13442.
- S19. D. Janardanan, D. Usharani, H. Chen and S. Shaik, *J. Phys. Chem. Lett.*, 2011, **2**, 2610.
- S20. (a) P. Winget, C. J. Cramer and D. G. Truhlar, *Theor. Chem. Acc.*, 2004, **112**, 217; (b) A. Lewis, J. A. Bumpus, D. G. Truhlar and C. J. Cramer, *J. Chem. Edu.*, 2004, **81**, 596.
- S21. D. Mandal, R. Ramanan, D. Usharani, D. Janardanan, B. Wang and S. Shaik, *J. Am. Chem. Soc.*, 2015, **137**, 722.

Energies

Table S3. $[\text{Fe}^{\text{IV}}\text{O}(\text{N4Py})]^{2+}$ in kcal mol⁻¹.

	Δlacvp	Δlacv3p^{*+}	$\Delta\mathbf{E}^a$	ΔZ_0	$\Delta\text{E(Thermal)}^b$	$-\text{T}\Delta\text{S}^b$	$\Delta\text{Dispersion}$	$\Delta\mathbf{G}^c$
$^3[\text{Fe}^{\text{IV}}\text{O}(\text{N4Py})]^{2+}$	0.00	+0.00	0.00	+0.00	+0.00	+0.00	+0.00	0.00
$^5[\text{Fe}^{\text{IV}}\text{O}(\text{N4Py})]^{2+}$	14.05	-5.64	8.41	-1.55	+0.68	-2.68	+2.01	6.87

^a Sum of the three previous columns. ^b T = 298.15 K. ^c Sum of the five previous columns.

Table S4. $[\text{Mn}^{\text{IV}}\text{O}(\text{N4Py})]^{2+}$ in kcal mol⁻¹.

	Δlacvp	Δlacv3p^{*+}	$\Delta\mathbf{E}^a$	ΔZ_0	$\Delta\text{E(Thermal)}^b$	$-\text{T}\Delta\text{S}^b$	$\Delta\text{Dispersion}$	$\Delta\mathbf{G}^c$
$^2[\text{Mn}^{\text{IV}}\text{O}(\text{N4Py})]^{2+}$	12.02	-0.40	11.45	-0.17	+0.10	+0.08	-0.11	11.52
$^4[\text{Mn}^{\text{IV}}\text{O}(\text{N4Py})]^{2+}$	0.00	+0.00	0.00	+0.00	+0.00	+0.00	+0.00	0.00
$^4[\text{Mn}^{\text{IV}}\text{O}(\text{N4Py})]^{2+ d}$	19.04	-3.28	15.76	-2.37	+1.00	-3.69	-0.16	10.55
$^6[\text{Mn}^{\text{IV}}\text{O}(\text{N4Py})]^{2+}$	32.73	-1.56	31.17	-2.10	+0.86	-2.95	-0.04	26.93

^a Sum of the three previous columns. ^b T = 298.15 K. ^c Sum of the five previous columns.

^d The excited state configuration $[\delta^{(1)}, \pi^*_{yz}^{(1)}, \pi^*_{xz}^{(0)}, \sigma^*_{xy}^{(1)}]$.

Table S5. $[\text{Fe}^{\text{IV}}\text{O}(\text{N4Py})]^{2+}$ with 1,4-cyclohexadiene in kcal mol^{-1} .

	ΔIacvp	ΔIacv3p^{*+}	$\Delta\mathbf{E}^a$	ΔZ_0	$\Delta\mathbf{E}(\text{Thermal})^b$	$-\text{T}\Delta\mathbf{S}^b$	$\Delta\text{Dispersion}$	$\text{RTln}(24.5)^{b,c}$	$\Delta\mathbf{G}^d$
S = 1									
Reactants, separated	1.33	-1.11	0.22	-0.20	-0.92	-7.91	+4.31	+1.89	-2.61
Reactants, complexed	0.00	+0.00	0.00	+0.00	+0.00	+0.00	+0.00		0.00
Transition state	10.10	+3.33	13.43	-3.42	-0.64	+3.87	-4.57		8.67
Intermediate	-13.49	-0.99	-14.48	-1.66	+0.13	-0.33	-1.94		-18.28
S = 2									
Reactants, separated	15.38	-6.75	8.63	-1.76	-0.24	-10.58	+6.32	+1.89	4.26
Reactants, complexed	13.88	-5.75	8.14	-1.46	+0.69	-2.80	+2.01		6.57
Transition state	17.19	-4.85	12.34	-3.65	+0.26	-0.44	+1.39		9.90
Intermediate	-7.62	-7.11	-14.73	-4.08	+1.09	-2.41	-0.74		-20.88

^a Sum of the three previous columns. ^b T = 298.15 K. ^c Correction for change of standard state for complexation in solvent. ^d Sum of the six previous columns.

Table S6. $[\text{Mn}^{\text{IV}}\text{O}(\text{N4Py})]^{2+}$ with 1,4-cyclohexadiene in kcal mol⁻¹.

	Δlacvp	Δlacv3p^{*+}	$\Delta\mathbf{E}^a$	ΔZ_0	$\Delta\mathbf{E}(\text{Thermal})^b$	$\Delta\text{Dispersion}$	$-\text{T}\Delta\mathbf{S}^b$	$\text{RTln}(24.5)^{b,c}$	$\Delta\mathbf{G}^d$
$S = 1/2$									
Reactants, separated	13.87	-2.00	11.87	-0.48	-0.77	+5.38	-8.55	+1.89	9.34
Reactants, complexed	12.67	-0.98	11.69	-0.27	+0.18	+0.97	-1.03		11.53
Transition state	14.59	+1.63	16.22	-2.16	-0.57	-2.09	+2.71		14.12
Intermediate	-9.45	-0.96	-10.41	-2.21	+0.24	-0.59	-0.11		-13.08
$S = 3/2$									
Reactants, separated	1.85	-1.59	0.26	-0.31	-0.87	+5.49	-8.63	+1.89	-2.18
Reactants, complexed	0.00	+0.00	0.00	+0.00	+0.00	+0.00	+0.00		0.00
$[\sigma_{\text{CH}}(\alpha) \rightarrow \sigma_{z_2}^* \rightarrow \sigma_{xy}^*]$									
Transition state	18.88	+1.67	20.55	-4.73	-0.13	+0.33	+0.59		16.60
Intermediate	-9.01	-5.38	-14.39	-3.40	+0.84	-0.75	-2.27		-19.98
$[\sigma_{\text{CH}}(\beta) \rightarrow \pi_{xz}^* \rightarrow \delta]$									
Transition state	17.50	+2.24	19.74	-3.88	-0.48	-1.22	+2.13		16.28
Intermediate	-9.28	-1.22	-10.50	-2.08	+0.24	+0.13	-0.41		-12.62
$[\pi_{xz}^*(\alpha) \rightarrow \sigma_{xy}^*, \sigma_{\text{CH}}(\alpha) \rightarrow \pi_{xz}^*]$									
Reactants, separated	20.89	-4.87	16.02	-2.68	+0.13	+5.33	-12.32	+1.89	8.37
Reactants, complexed ^e	18.87	-3.61	15.26	-2.27	+0.44	-0.18	-2.30		10.96

^a Sum of the three previous columns. ^b T = 298.15 K. ^c Correction for change of standard state for complexation in solvent. ^d Sum of the six previous columns. ^e Estimated value obtained from a semi-stable point during optimizations, which ultimately ends up either in the reactant ground state configuration, or directly to the H-atom abstracted intermediate.

Table S7. $[\text{Fe}^{\text{IV}}\text{O}(\text{N4Py})]^{2+}$ with thioanisole in kcal mol⁻¹.

	Δlacvp	Δlacv3p^{*+}	ΔE^a	ΔZ_0	$\Delta E(\text{Thermal})^b$	$-\text{T}\Delta S^b$	$\Delta\text{Dispersion}$	$\text{RTln}(24.5)^{b,c}$	ΔG^d
S = 1									
Reactants, separated	1.48	-0.70	0.77	-0.17	-0.87	+5.36	-6.82	+1.74	0.01
Reactants, complexed	0.00	+0.00	0.00	+0.00	+0.00	+0.00	+0.00		0.00
Reactants, complexed π	22.18	-3.78	18.40	-1.76	+0.48	-3.87	+0.72		13.98
Transition state	23.17	-3.49	19.68	-2.21	+0.14	-4.01	+1.67		15.27
Product	-5.07	+1.16	-3.92	-1.04	+0.11	-1.03	+1.25		-4.63
S = 2									
Reactants, separated	14.60	-5.47	9.13	-1.70	-0.24	+7.36	-9.17	+1.74	7.12
Reactants, complexed	13.18	-4.76	8.42	-1.40	+0.60	+2.04	-1.85		7.81
Transition state	16.29	-5.80	10.49	-2.04	+0.26	-1.42	+0.35		7.64
Product	-16.71	-2.84	-19.56	-1.90	+0.59	-0.82	-0.09		-21.77

^a Sum of the three previous columns. ^b T = 273.15 K. ^c Correction for change of standard state for complexation in solvent. ^d Sum of the six previous columns.

Table S8. $[\text{Mn}^{\text{IV}}\text{O}(\text{N4Py})]^{2+}$ with thioanisole in kcal mol⁻¹.

	ΔIacvp	ΔIacv3p^{*+}	$\Delta\mathbf{E}^a$	ΔZ_0	$\Delta\mathbf{E}(\text{Thermal})^b$	$\Delta\text{Dispersion}$	$-\text{T}\Delta\mathbf{S}^b$	$\text{RTln}(24.5)^{b,c}$	$\Delta\mathbf{G}^d$
<i>S = 1/2</i>									
Reactants, separated	11.66	+0.64	12.29	-0.18	-0.80	+5.46	-6.87	+1.74	11.64
Reactants, complexed	10.25	+1.35	11.60	-0.12	+0.12	-0.10	-0.45		11.06
Transition state	18.98	+0.51	19.49	-0.64	-0.64	-4.01	+4.61		18.80
Product	3.45	+2.32	5.76	+0.10	-0.48	-2.88	+3.75		6.26
<i>S = 3/2</i>									
<i>[\sigma_{\text{CH}}(\alpha) \rightarrow \sigma^*_{z^2}]</i>									
Reactants, separated	1.65	-0.84	0.81	-0.16	-0.88	+5.58	-6.97	+1.74	0.12
Reactants, complexed	0.00	+0.00	0.00	+0.00	+0.00	+0.00	+0.00		0.00
Transition state	25.96	-0.97	24.99	-1.16	-0.42	-2.32	+3.50		24.58
Product	2.20	+1.43	3.63	-0.87	+0.00	-3.40	+1.92		1.28
<i>[\sigma_{\text{CH}}(\alpha) \rightarrow \pi^*_{xz}]</i>									
Reactants, separated									
Reactants, complexed	12.72	-3.47	9.25	-1.63	+0.49	-2.88	+0.24		5.48
Transition state	21.37	-2.87	18.50	-1.99	+0.08	-2.57	+1.45		15.47
Product	8.36	+0.18	8.54	-1.19	+0.21	-2.12	+1.07		6.51
MECP	19.95	-4.90	15.06						
<i>S = 5/2</i>									
Reactants, separated	36.76	-4.64	32.12	-2.23	-0.11	+5.60	-9.52	+1.74	27.60
Reactants, complexed	26.64	-4.61	22.03	-2.46	+0.59	-0.07	-0.84		19.25
Transition state	27.64	-4.54	23.11	-2.63	+0.19	+0.05	-0.04		20.67
Product	-22.64	-2.38	-25.01	-1.67	+0.48	-0.66	+0.31		-26.56
MECP	19.96	-4.66	15.30						

^a Sum of the three previous columns. ^b T = 273.15 K. ^c Correction for change of standard state for complexation in solvent. ^d Sum of the six previous columns.

Mulliken Spin Density Distribution

Table S9. $[\text{Fe}^{\text{IV}}\text{O}(\text{N4Py})]^{2+}$.

	Fe	O	5 x ligated N	Rest
$^3[\text{Fe}^{\text{IV}}\text{O}(\text{N4Py})]^{2+}$	1.30	0.91	-0.14	-0.07
$^5[\text{Fe}^{\text{IV}}\text{O}(\text{N4Py})]^{2+}$	3.08	0.72	0.12	0.09

Table S10. $[\text{Mn}^{\text{IV}}\text{O}(\text{N4Py})]^{2+}$.

	Mn	O	5 x ligated N	Rest
$^2[\text{Mn}^{\text{IV}}\text{O}(\text{N4Py})]^{2+}$	1.06	0.04	-0.13	0.03
$^4[\text{Mn}^{\text{IV}}\text{O}(\text{N4Py})]^{2+}$	2.56	0.69	-0.43	0.18
$^4[\text{Mn}^{\text{IV}}\text{O}(\text{N4Py})]^{2+ a}$	3.60	-0.70	-0.14	0.24
$^6[\text{Mn}^{\text{IV}}\text{O}(\text{N4Py})]^{2+}$	4.08	1.08	-0.31	0.15

^a The excited state configuration $[\delta^{(1)}, \pi^*_{yz}{}^{(1)}, \pi^*_{xz}{}^{(0)}, \sigma^*_{xy}{}^{(1)}]$.

Table S11. $[\text{Fe}^{\text{IV}}\text{O}(\text{N4Py})]^{2+}$ with 1,4-cyclohexadiene.

	Fe	O	5 x ligated N	Substrate	Rest
$S = 1$					
Reactants, complexed	1.21	0.91	-0.10	0.00	-0.03
Transition state	0.99	0.71	-0.10	0.40	-0.01
Intermediate	0.99	0.16	-0.15	0.98	0.02
$S = 2$					
Reactants, complexed	3.10	0.71	0.12	0.00	0.07
Transition state	3.57	0.41	0.17	-0.23	0.07
Intermediate	4.07	0.40	0.35	-0.97	0.14

Table S12. $[\text{Mn}^{\text{IV}}\text{O}(\text{N4Py})]^{2+}$ with 1,4-cyclohexadiene.

	Mn	O	5 x ligated N	Substrate	Rest
$S = 1/2$					
Reactants, complexed	1.07	0.04	-0.13	0.00	0.03
Transition state	1.76	-0.28	-0.23	-0.28	0.03
Intermediate	2.06	0.15	-0.26	-0.98	0.03
$S = 3/2$					
Reactants, complexed	2.56	0.71	-0.44	0.00	0.16
$[\sigma_{\text{CH}}(\alpha) \rightarrow \sigma_{z^2}^* \rightarrow \sigma_{xy}^*]$					
Transition state	3.44	0.15	-0.36	-0.38	0.14
Intermediate	4.00	0.10	-0.30	-0.98	0.18
$[\sigma_{\text{CH}}(\beta) \rightarrow \pi_{xz}^* \rightarrow \delta]$					
Transition state	2.31	0.60	-0.36	0.31	0.14
Intermediate	2.06	0.17	-0.27	1.00	0.03
$[\pi_{xz}^*(\alpha) \rightarrow \sigma_{xy}^*, \sigma_{\text{CH}}(\alpha) \rightarrow \pi_{xz}^*]$					
Reactants, complexed	3.70	-0.72	-0.20	-0.01	0.23

Table S13. $[\text{Fe}^{\text{IV}}\text{O}(\text{N4Py})]^{2+}$ with thioanisole.

	Mn	O	5 x ligated N	Substrate	Rest
S = 1					
Reactants, complexed	1.20	0.92	-0.10	0.00	-0.02
Reactants, complexed II	2.60	-0.01	-0.06	-0.53	0.01
Transition state	2.48	0.07	-0.07	-0.48	0.00
Product	2.06	0.02	-0.10	0.01	0.02
S = 2					
Reactants, complexed	3.11	0.72	0.11	0.00	0.06
Transition state	3.57	0.49	0.13	-0.24	0.06
Product	3.72	0.06	0.06	0.04	0.12

Table S14. $[\text{Mn}^{\text{IV}}\text{O}(\text{N4Py})]^{2+}$ with thioanisole.

	Mn	O	5 x ligated N	Substrate	Rest
S = 1/2					
Reactants, complexed	0.96	0.13	-0.11	0.00	0.02
Transition state	1.54	0.03	-0.17	-0.39	-0.01
Product	1.19	0.01	-0.18	0.00	-0.02
S = 3/2					
[$\sigma_{\text{CH}(\alpha)} \rightarrow \sigma^*_{z_2}$]					
Reactants, complexed	2.55	0.71	-0.42	0.00	0.16
Transition state	2.38	0.28	-0.19	0.56	-0.03
Product	3.26	0.01	-0.25	0.01	-0.03
[$\sigma_{\text{CH}(\alpha)} \rightarrow \pi^*_{xz}$]					
Reactants, complexed	3.67	-0.26	-0.21	-0.43	0.23
MECP	3.72	-0.11	-0.24	-0.58	0.21
Transition state	3.51	0.01	-0.31	-0.40	0.20
Product	3.17	0.01	-0.31	0.01	0.11
S = 5/2					
Reactants, complexed	3.83	0.31	-0.27	0.97	0.17
Transition state	3.79	0.36	-0.24	0.91	0.18
MECP	4.11	0.32	-0.20	0.61	0.16
Product	4.91	0.02	-0.22	0.02	0.27

Geometries

Table S15. $[\text{Fe}^{\text{IV}}\text{O}(\text{N4Py})]^{2+}$ distances (Å).

	D(Fe-O)	D(Fe-N _{ax})	D(Fe-N _{eq1})	D(Fe-N _{eq2})	D(Fe-N _{eq3})	D(Fe-N _{eq4})
$^3[\text{Fe}^{\text{IV}}\text{O}(\text{N4Py})]^{2+}$	1.66	2.06	1.99	1.99	1.97	1.97
$^5[\text{Fe}^{\text{IV}}\text{O}(\text{N4Py})]^{2+}$	1.65	2.08	2.13	2.13	2.08	2.09

Table S16. $[\text{Mn}^{\text{IV}}\text{O}(\text{N4Py})]^{2+}$ distances (Å).

	D(Mn-O)	D(Mn-N _{ax})	D(Mn-N _{eq1})	D(Mn-N _{eq2})	D(Mn-N _{eq3})	D(Mn-N _{eq4})
$^2[\text{Mn}^{\text{IV}}\text{O}(\text{N4Py})]^{2+}$	1.61	2.12	2.02	2.02	2.01	2.01
$^4[\text{Mn}^{\text{IV}}\text{O}(\text{N4Py})]^{2+}$	1.67	2.12	2.02	2.02	2.00	2.00
$^4[\text{Mn}^{\text{IV}}\text{O}(\text{N4Py})]^{2+ a}$	1.72	2.11	2.30	2.09	2.07	2.18
$^6[\text{Mn}^{\text{IV}}\text{O}(\text{N4Py})]^{2+}$	1.90	2.10	2.31	2.04	2.02	2.25

^a The excited state configuration $[\delta^{(1)}, \pi^*_{yz}{}^{(1)}, \pi^*_{xz}{}^{(0)}, \sigma^*_{xy}{}^{(1)}]$.

Table S17. $[\text{Fe}^{\text{IV}}\text{O}(\text{N4Py})]^{2+}$ with 1,4-cyclohexadiene distances and angles (\AA and $^\circ$).

	D(Fe-O)	D(Fe-N _{ax})	D(Fe-N _{eq1})	D(Fe-N _{eq2})	D(Fe-N _{eq3})	D(Fe-N _{eq4})	D(O-H)	D(FeOH-C ₆ H ₇)	A(Fe-O-H)
S = 1									
Reactants, complexed	1.66	2.06	1.99	1.99	1.97	1.97	2.65	1.10	153.55
Transition state	1.75	2.05	1.99	1.99	1.98	1.98	1.39	1.25	124.46
Intermediate	1.82	2.03	1.99	1.99	1.98	1.97	0.98	2.47	116.55
S = 2									
Reactants, complexed	1.65	2.08	2.14	2.13	2.08	2.09	2.57	1.10	151.37
Transition state	1.69	2.18	2.15	2.16	2.12	2.11	1.65	1.15	165.73
Intermediate	1.79	2.27	2.18	2.18	2.15	2.13	0.98	2.18	160.81

Table S18. $[\text{Mn}^{\text{IV}}\text{O}(\text{N4Py})]^{2+}$ with 1,4-cyclohexadiene distances and angles (\AA and $^\circ$).

	D(Mn-O)	D(Mn-N _{ax})	D(Mn-N _{eq1})	D(Mn-N _{eq2})	D(Mn-N _{eq3})	D(Mn-N _{eq4})	D(O-H)	D(MnOH-C ₆ H ₇)	A(Mn-O-H)
S = 1/2									
Reactants, complexed	1.61	2.13	2.02	2.02	2.01	2.01	2.65	1.10	143.08
Transition state	1.70	2.10	2.03	2.02	2.02	2.02	1.62	1.16	124.51
Intermediate	1.80	2.07	2.03	2.03	2.01	2.01	0.98	2.33	124.75
S = 3/2									
Reactants, complexed	1.68	2.12	2.02	2.02	2.00	2.00	2.65	1.10	158.85
$[\sigma_{\text{CH}}(\alpha) \rightarrow \sigma_{z^2}^* \rightarrow \sigma_{xy}^*]$									
Transition state	1.77	2.26	2.05	2.05	2.03	2.03	1.27	1.29	169.51
Intermediate	1.80	2.11	2.34	2.07	2.05	2.23	0.98	2.29	124.69
$[\sigma_{\text{CH}}(\beta) \rightarrow \pi_{xz}^* \rightarrow \delta]$									
Transition state	1.76	2.10	2.02	2.03	2.01	2.01	1.34	1.27	128.04
Intermediate	1.80	2.07	2.03	2.03	2.01	2.01	0.98	2.39	125.14
$[\pi_{xz}^*(\alpha) \rightarrow \sigma_{xy}^*, \sigma_{\text{CH}}(\alpha) \rightarrow \pi_{xz}^*]$									
Reactants, complexed	1.72	2.11	2.10	2.28	2.18	2.07	2.64	1.10	164.33

Table S19. $[\text{Fe}^{\text{IV}}\text{O}(\text{N4Py})]^{2+}$ with thioanisole distances and angles (\AA and $^\circ$).

	D(Fe-O)	D(Fe-N _{ax})	D(Fe-N _{eq1})	D(Fe-N _{eq2})	D(Fe-N _{eq3})	D(Fe-N _{eq4})	D(O-S)	A(Fe-O-S)
S = 1								
Reactants, complexed	1.63	2.07	1.99	1.99	1.97	1.98	4.39	142.05
Reactants, complexed II	1.67	2.12	2.03	2.34	2.24	2.03	2.35	131.64
Transition state	1.71	2.12	2.02	2.34	2.25	2.02	2.08	132.79
Product	2.16	2.21	2.01	2.12	2.09	1.99	1.56	131.07
S = 2								
Reactants, complexed	1.62	2.09	2.14	2.12	2.08	2.09	4.01	154.44
Transition state	1.66	2.20	2.17	2.16	2.12	2.12	2.72	167.37
Product	2.05	2.26	2.25	2.24	2.21	2.20	1.57	129.74

Table S20. $[\text{Mn}^{\text{IV}}\text{O}(\text{N4Py})]^{2+}$ with thioanisole distances and angles (\AA and $^\circ$).

	D(Mn-O)	D(Mn-N _{ax})	D(Mn-N _{eq1})	D(Mn-N _{eq2})	D(Mn-N _{eq3})	D(Mn-N _{eq4})	D(O-S)	A(Mn-O-S)
S = 1/2								
Reactants, complexed	1.59	2.14	2.03	2.02	2.01	2.01	4.18	146.27
Transition state	1.78	2.09	2.05	2.04	2.04	2.04	1.91	131.84
Product	2.05	2.05	2.06	2.05	2.03	2.03	1.57	127.13
S = 3/2								
[$\sigma_{\text{CH}(\alpha)} \rightarrow \sigma^*_{z_2}$]								
Reactants, complexed	1.65	2.13	2.02	2.02	2.00	2.00	4.45	137.67
Transition state	1.79	2.16	2.06	2.06	2.03	2.03	1.94	165.49
Product	2.20	2.30	2.07	2.07	2.06	2.06	1.56	133.73
[$\sigma_{\text{CH}(\alpha)} \rightarrow \pi^*_{xz}$]								
Reactants, complexed	1.69	2.16	2.22	2.24	2.19	2.16	2.47	133.48
MECP	1.74	2.18	2.20	2.28	2.24	2.16	2.16	151.14
Transition state	1.79	2.13	2.40	2.11	2.10	2.30	1.87	134.60
Product	2.06	2.12	2.42	2.06	2.08	2.30	1.56	131.96
S = 5/2								
Reactants, complexed	1.69	2.20	2.30	2.21	2.17	2.22	4.09	143.78
Transition state	1.70	2.19	2.22	2.30	2.22	2.16	3.28	167.99
MECP	1.74	2.18	2.20	2.28	2.24	2.16	2.16	151.14
Product	2.15	2.36	2.32	2.32	2.27	2.27	1.56	128.60

C 1.34435 4.55817 6.28946
C 2.18512 3.44511 6.19899
C 3.53539 3.62925 5.87778
C 4.49938 2.45802 5.86373
C 5.38945 2.12225 3.57028
C 4.77192 3.14986 2.64203
C 3.94427 2.75863 1.58286
C 3.45958 3.72629 0.69813
C 3.80525 5.06851 0.89650
C 4.62083 5.39419 1.97910
H 6.98872 6.03463 7.88320
H 7.86470 5.00703 9.99439
H 8.31375 2.53798 10.03240
H 7.87623 1.19380 7.96749
H 6.99631 1.10803 5.68136
H 9.17197 0.71363 4.63970
H 10.99639 1.53268 3.13578
H 10.87295 3.87390 2.23925
H 8.92173 5.30607 2.88679
H 3.67741 6.90493 5.50308
H 1.24762 6.71826 6.10793
H 0.29681 4.43204 6.53789
H 1.80315 2.44620 6.37530
H 3.68572 1.71353 1.45755

H 2.81835 3.43864 -0.12712
H 3.44449 5.84594 0.23464
H 4.90215 6.41666 2.19791
H 3.95721 1.53734 5.61582
H 4.88159 2.32703 6.88131
H 4.74856 1.23314 3.61737
H 6.33792 1.79822 3.12984
S 7.01549 8.17951 4.99702
C 8.35683 8.38443 3.80495
C 9.60598 8.79742 4.28616
C 10.66345 8.95697 3.38181
C 10.47005 8.68889 2.02086
C 9.21842 8.26123 1.55450
C 8.15176 8.10662 2.44680
H 9.75526 8.99070 5.34350
H 11.63391 9.27963 3.74201
H 11.29341 8.80671 1.32482
H 9.07301 8.04908 0.50096
H 7.18416 7.76566 2.09637
C 6.07191 9.70234 4.67035
H 5.18791 9.68279 5.31056
H 6.69514 10.56382 4.91967
H 5.78271 9.72602 3.61761

67
MECP (2/4) or (2/6)
Mn 6.68469 4.54350 4.30309
N 5.86118 2.58029 4.77466
N 6.17889 4.72477 6.43820
N 8.45561 3.39806 5.16699
N 4.54929 4.77672 3.67088
N 6.97870 3.54106 2.41167
O 7.39868 6.10230 3.98103
C 5.91441 5.84240 7.14932
C 5.56128 5.77755 8.49991
C 5.47906 4.52638 9.11935
C 5.75953 3.36907 8.37987
C 6.10942 3.50566 7.03817
C 6.50586 2.34538 6.13378
C 8.01856 2.38599 5.95997
C 8.90073 1.51601 6.59757
C 10.27718 1.70664 6.41248
C 10.72389 2.75229 5.59752
C 9.87106 3.58088 4.98283
C 4.05692 5.78214 2.90899
C 2.76709 5.74291 2.38076
C 1.97113 4.61919 2.63329
C 2.48278 3.57764 3.41377

C 3.77708 3.68977 3.93016
C 4.35731 2.65746 4.86632
C 6.30544 1.58545 3.72971
C 6.62116 2.23094 2.39980
C 6.61292 1.49717 1.20930
C 6.99486 2.12476 0.01993
C 7.37361 3.47293 0.04553
C 7.34741 4.15330 1.26052
H 5.99548 6.78213 6.61887
H 5.35411 6.68764 9.04846
H 5.19821 4.44877 10.16298
H 5.70430 2.38732 8.83439
H 6.19061 1.39022 6.56428
H 8.52503 0.71289 7.22026
H 10.98706 1.04648 6.89639
H 11.78131 2.92363 5.43845
H 10.07008 4.40208 4.33917
H 4.72305 6.61431 2.72836
H 2.39969 6.56656 1.78173
H 0.96912 4.55404 2.22574
H 1.88912 2.69493 3.62127
H 6.31332 0.45585 1.21680
H 6.99257 1.57309 -0.91275
H 7.67526 3.98729 -0.85772

H 7.61401 5.19781 1.34342
H 3.91790 1.67196 4.68295
H 4.09260 2.93622 5.89075
H 5.54230 0.81152 3.60522
H 7.20666 1.08230 4.09302
S 7.45970 7.96743 2.89088
C 6.83077 9.12269 4.06902
C 5.54545 9.64381 3.80684
C 4.95949 10.53110 4.71168
C 5.64367 10.90269 5.87753
C 6.91925 10.38253 6.13664
C 7.51614 9.49001 5.24236
H 5.01878 9.36815 2.89944
H 3.97512 10.93519 4.50359
H 5.18660 11.59202 6.57888
H 7.45187 10.66884 7.03672
H 8.49830 9.09158 5.46199
C 9.25946 7.99869 3.12305
H 9.67404 7.30845 2.38664
H 9.63952 9.00638 2.94398
H 9.51529 7.65070 4.12337